Scattered Visible and Ultraviolet Solar Radiation from Condensed Attitude Control Jet Plumes

C.E. Kolb* and R.B. Lyons†
Aerodyne Research, Inc., Billerica, Massachusetts
and
J.B. Elgin‡
Physical Sciences, Inc., Woburn, Massachusetts
and
R.E. Huffman,§ D.E. Paulsen,¶ and A. McIntyre**
Air Force Geophysics Laboratory, Hanscom Air Force Base, Bedford, Massachusetts

Strong ultraviolet and visible radiation signals due to solar scattering from attitude control system (ACS) plumes associated with a space platform have been observed and analyzed. The analysis presented confirms that the observed signals are caused by condensed droplets of argon, the propellant for the ACS jets. The analysis predicts very similar signals for equivalent ACS jets using nitrogen as a propellant. However, scattered signals for jets employing neon as a propellant are predicted to be more than two orders of magnitude smaller than those from Ar or N_2 ACS jet plumes.

Nomenclature

A = cross-sectional area in nozzle
C = cluster flow rate
C_{FR} = ratio of vacuum thrust coefficient to its maximum value $= \frac{(1+\cos\eta)}{2}\frac{V_E}{V_t}\left(1+\frac{1}{\gamma_E M_E^2}\right)$
d = nozzle throat diameter
D = mean cluster diameter
$I(\lambda)$ = solar flux
l = mean free path
m = refractive index
$\dot{m}$ = mass flow rate
M = Mach number
n = Ar cluster concentration
$\bar{N}$ = mean number of Ar atoms per cluster
P = pressure
Q_{scat} = ratio of single cluster scattering cross section to its geometric cross section
r = radial coordinate in spherical polar coordinate system
T = temperature
V = velocity
x = particle size parameter $= \pi D/\lambda$
γ = ratio of specific heats
η = nozzle cone half-angle
θ = solar scattering angle
λ = photon wavelength
ζ = Brook model plume angular distribution parameter $= (1 - C_{FR}^{-1})$
ρ = density
ϕ = polar angle in a spherical polar coordinate system

Subscripts

eq = equivalent
e = exit plane
0 = stagnation point
pitch = pitch attitude control jet
SJ = settling jet
T = thermal

Received March 8, 1982; revision received Jan. 3, 1983.

*Director, Applied Sciences Division.
†Senior Research Scientist, Applied Sciences Division, Center for Chemical and Environmental Physics. Member AIAA.
‡Principal Scientist; presently with Spectral Sciences, Inc.
§Supervisory Research Chemist, Aeronomy Division. Member AIAA.
¶Research Chemist, Aeronomy Division.
**Program Manager, Optical Physics Division.

Introduction

SPACE-borne advanced optical systems may be sensitive to optical contamination of their local environment by gases and/or particles produced by off-gasing of platform components or by operation of attitude control system (ACS) jets and orientation rocket motors. These "self-interference" phenomena may be due to the direct emission of radiation from relatively hot molecules produced by the space platform components, from "atmospheric interaction" radiation produced when optically active contaminant molecules are excited in inelastic or chemiluminescent collisions with ambient atmospheric species, or from solar or earthshine radiation scattered by contaminant molecules or particles.

The direct emission and atmospheric interaction mechanisms are of primary importance to infrared optical systems. The atmospheric interaction mechanism produces a more troublesome extended source, and has been previously evaluated for a variety of high-attitude rocket engine and ACS jet exhaust plumes.[1-5] The effect of both direct emission and atmospheric interaction radiation from contaminant molecules on a sensitive space-shuttle-borne IR telescope has been investigated.[6]

In this article, we report the observation and analysis of very significant visible and uv interference signals caused by solar radiation scattered from condensed ACS jet exhaust gases. Solar radiation scattered by these particulates and by optically active molecules is probably the most serious source of contamination induced interference for visible and uv space borne optical systems. An analysis of the scattering of IR and uv solar radiation from optically active molecules in typical rocket exhaust plumes has recently been published.[7]

Previous observations and analyses of visible signals from the translunar injection burn of the Saturn IV B spacecraft during the Apollo 8 mission have indicated that condensed exhaust plume water vapor could produce large solar scat-

tering signals.[8,9] The observations reported and analyzed here demonstrate that particulates formed in ACS jet plumes of the transparent gases Ar and N_2 can be a very serious source of contaminant interference radiation readily observable by sensitive visible and uv space-borne optical systems.

Experiment and Instrumentation Description

As part of the AFGL's Multispectral Measurements Program (MSMP), quantitative uv measurements as well as qualitative visible observations were made of interference radiation due to argon propelled ACS and settling (ullage) jets on a space platform at altitudes ranging from approximately 150 to 240 km.

The MSMP experiment reported here (TEM-2) consisted of a target module, which contained pairs of argon propelled pitch, roll, and yaw ACS jets as well as a set of argon propelled settling jets for a small liquid fueled rocket motor, and a sensor module, which contained uv, visible, and IR sensors used to monitor the optical signatures associated with the target platform operation. The target and sensor modules were co-launched aboard an Aries booster from White Sands Missile Range in the spring of 1980. The slant range between the sensor and target platforms varied between 0.5 and 10 km for the observations reported here. These observations were made in full daylight, with a sun-target-sensor angle of approximately 90 deg.

Characteristics of the target module ACS and settling jets are presented in Table 1.

The propellant used during the MSMP TEM-2 flight in the ACS and settling jets was prepurified argon with a stated purity of 99.998%. The moisture content of the argon propellant was certified at less than 3 ppm.

The target module ACS jets were operated in a modulated pulse width mode, with a pulsing rate for the target module ACS of 10 pulses/s. The target module settling jets fired continuously for 5 s before each rocket engine burn.

Measurements in the vacuum-uv/uv wavelength region were made with spatially resolving photometers using digicon image tubes. Two photometers were used: the high sensitivity photometer, HSP-53, in the vacuum ultraviolet; and the medium sensitivity photometer, MSP-33, in the ultraviolet. They each use 10×10 pixel (picture element) square arays in the digicon detectors. Wavelength band isolation was obtained using interference filters, window transmission limits, and solar blind photocathodes. Filter sensitivity curves for the four bandpasses used with each instrument are shown in Figs. 1 and 2. More complete descriptions of these instruments and their calibration may be found in Ref. 10 and 11.

Visible motion pictures of the jet interference radiation were made with a television recording system utilizing an RCA Type V vidicon tube employing an f/.78 lens system with a 25 mm focal length. Visible still photographs were obtained with a 35 mm camera equipped with an f/2.0 lens system with a 135 mm focal length and utilizing Kodak 2575 Recording film. Analysis of the visible vidicon data allowed independent confirmation of ACS and settling jet activity, tying the uv and vacuum-uv photometer observations clearly to the spatially and directionally resolved firing of the various cold gas jets on board the target platform.

Table 1 Target module ACS and settling jet source characteristics

	Cone half-angle, deg	Area ratio	Throat diameter, mm	Nominal source pressure, psia	Nominal source temp. K
Pitch, yaw ACS	15	47:1	4.8	212	300
Roll ACS	15	23:1	1.6	203	300
Settling jet	15	15.5:1	4.8	242	300

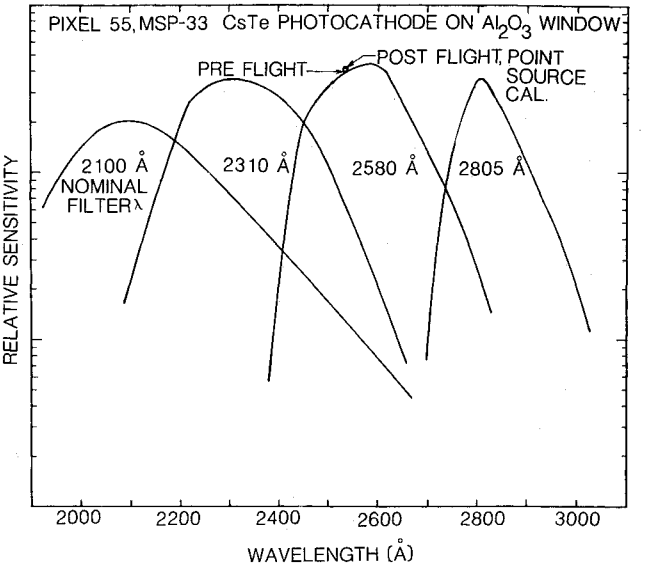

Fig. 1 HSP-53 sensitivity curves.

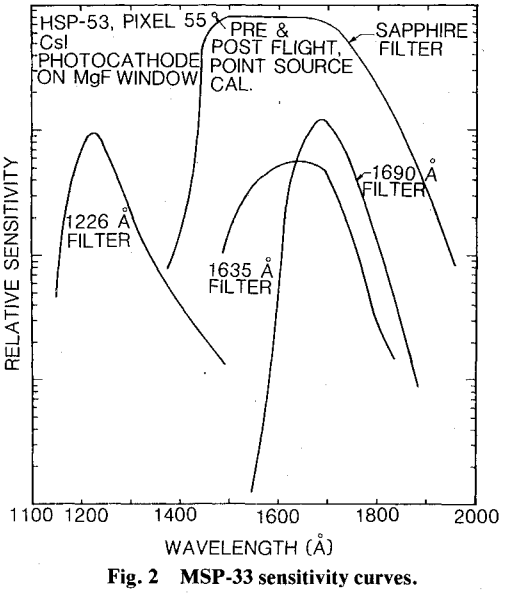

Fig. 2 MSP-33 sensitivity curves.

Observations

Pictures from the vidicon and the still camera aboard the target module revealed unexpectedly strong visible radiation structures associated with firings of the target module ACS and settling jets. The one-to-one association of strong visible signals with these target module jets extended to data from the MSP and HSP photometers. Also, an uv movie prepared from the uv photometer data clearly showed well-developed plume-like structures associated with ACS and settling jet firings.

The plume-like structure of these jet-associated visible and uv interference signals is clearly shown in Fig. 3, which is a still photograph of the settling jet firing which preceded the first target module engine burn. This picture shows the "vacuum core"-like structure of the jet-associated signals. The overall shape of the plume structure, although distorted by target module translation and sunlight reflected from the target module body, is that expected for a high-altitude supersonic expansion. The radiation intensity is highest near the nozzle where the plume gases are densest. This strongly suggested that the observed signals are not due to any collisional processes arising from jet-atmospheric interactions.

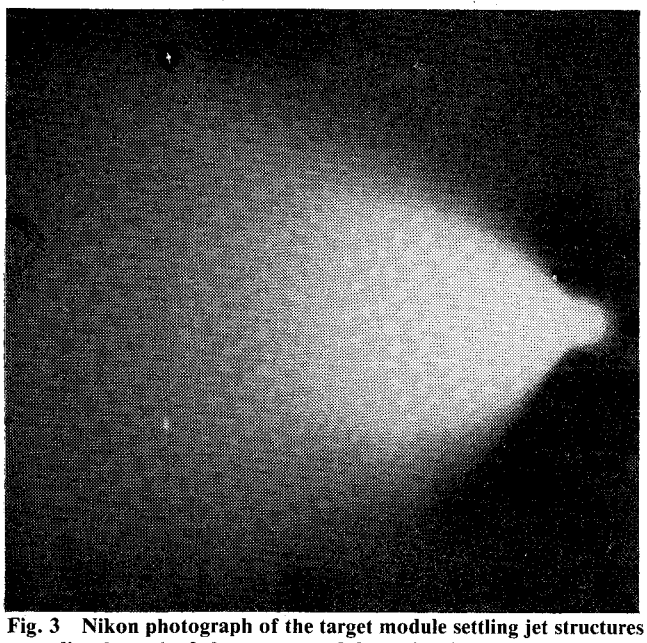

Fig. 3 Nikon photograph of the target module settling jet structures preceding burn 1 of the target module engine (bright streaks in the background are stellar images).

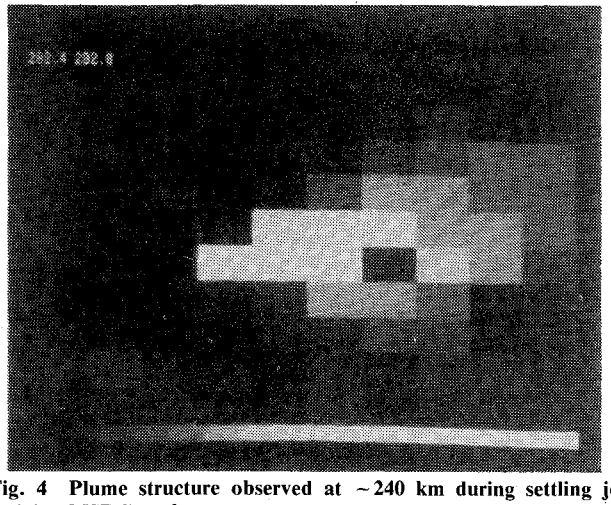

Fig. 4 Plume structure observed at ~240 km during settling jet activity, MSP filter 3.

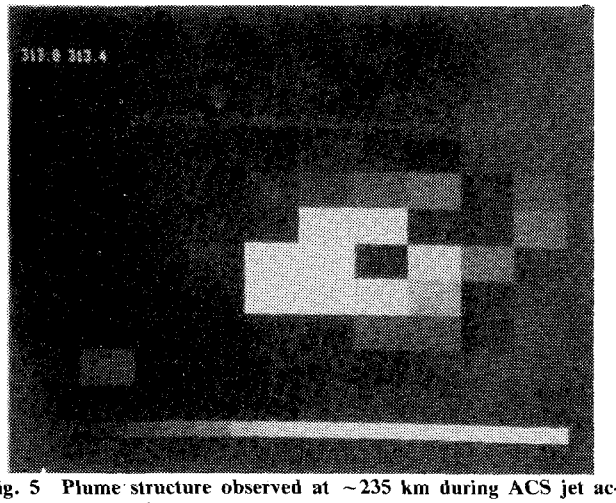

Fig. 5 Plume structure observed at ~235 km during ACS jet activity, MSP filter 3.

In order to visualize the time variation of the photometer data, video tapes of the pixel-by-pixel radiance were made for each filter using a 64-step gray scale. The result is a 10×10 matrix of squares, with each square representing one pixel. The magnitude of the spectral radiance is represented by the shade of gray, with lighter regions representing higher intensity. Examples of the two sets of plume images selected for detailed analysis are depicted in Figs. 4 and 5. The space platform with the jets is just to the left of center in each figure. The jet flowfield propagates in a direction that is perpendicular to the line of sight between target and sensor modules. The angle between the sun and sensor line of sight is about 90 deg, as noted above. An individual plume image was taken to consist of the same number of pixels for the different filters. The plume intensity was then taken as the sum of the calibrated counting rates for the relevant pixels multiplied by the projected area of a pixel field of view of the target.

Analysis of Argon Jet Radiation

The argon used as a propellant in the MSMP TEM-2 ACS and settling jets was sufficiently pure, and the observed visible and uv signals sufficiently strong, so that it would be very difficult to explain the data by involving some unknown impurity. Since the total expected impurity level is two parts in a hundred thousand, and the most probable impurities are N_2 and O_2, neither of which is strongly optically active, there appears to be no choice but to find a mechanism by which argon itself can cause the observed signals.

Gaseous Argon Radiation

An analysis of radiation mechanisms for the two most probable gaseous argon species, Ar and Ar_2, quickly showed that neither species can be responsible for the observed radiation. There are no allowed emission lines for Ar which radiate between 106.7 and 840.6 nm,[12] a consequence of the mere 4.14-eV gap between the lowest allowed excited state in Ar and its ionization potential at 15.76 eV. Thus monomeric Ar could not contribute significant radiation to any of the HSP or MSP filter bands, which cover the region from about 120 to 280 nm.

The situation is not significantly better for dimeric argon which might be formed during the nozzle expansion process. Ar_2 does have a broad $1u,\ 0u^-$ to $X^1\Sigma_g^+$ transition centered at about 126.0 nm.[13,14] However, observed emissions from this, the Ar_2 lowest excited state, are typically restricted to the 120.0-140.0 nm region.[13,14] Other known Ar_2 excited states lie within 1.5 eV of the $1u,\ 0u^-$ state, restricting their output to wavelengths less than 140 nm or greater than 800 nm. Thus Ar_2 cannot account for any radiation in the three longest wavelength HSP filter bands, any of the MSP filter bands, or for the visible vidicon or still pictures.

Argon Condensation Analysis

The remaining method by which Ar could cause the observed signatures requires condensation of the gaseous Ar into droplets of liquid or solid argon due to cooling during the nozzle expansion process. The boiling point of Ar at atmospheric pressure is 87.5 K, and its freezing point is 84.0 K. Its extremely narrow (3.5 K) liquid range indicates that condensation will quickly be followed by freezing into solid droplets.

The lowest temperature attainable in a freejet expansion can be calculated from the terminal Mach number of the expansion. Experimental measurements of argon jet properties and associated theoretical analyses for jet temperatures and Mach numbers have been published by Anderson and Fenn.[15] The terminal Mach number is defined by Anderson and Fenn for $\gamma = 5/3$ gases such as Ar by

$$M_T = 1.7(l/d_{eq})^{(1-\gamma)/\gamma} = 1.7(l/d_{eq})^{-0.4} \qquad (1)$$

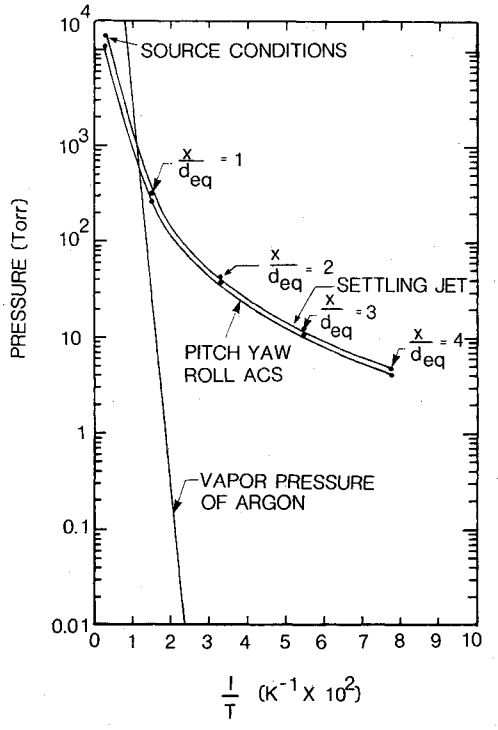

Fig. 6 Target module argon plume temperature profiles, X is the axial distance from the nozzle throat.

The ratio of l/d_{eq} represents a Knudsen number characteristic of the supersonic expansion process.

In order to apply Eq. (1) to the conical nozzles used on the target module it is necessary to relate the conical nozzle throat diameter to the diameter of an equivalent sonic nozzle. This relation is given by Hagena for $\gamma = 5/3$ gases as[16]

$$d_{eq} = 0.73 d \cot\eta \tag{2}$$

Using Eqs. (1) and (2), the terminal Mach number can be calculated for the settling and ACS jets. From the terminal Mach number, the terminal temperature can be calculated using the relation between beam temperature and Mach number:

$$T = T_0 \left(1 + \frac{\gamma - 1}{2} M^2\right)^{-1} \tag{3}$$

Using Eqs. (1-3) the terminal Mach numbers and centerline temperatures for all the target module argon jets were calculated to be above 100 and below 0.01 K, respectively. While there is no doubt that terminal conditions of this severity are not reached in a real expansion, there is little doubt that extremely high levels of supersaturation for Ar are clearly obtained in all of the target module jets. This can be dramatically demonstrated by calculation of the local jet centerline pressure, Mach number, and temperature according to Anderson and Fenn,[15] and comparing it to the argon vapor pressure as a function of temperature. Such a plot for the target module's settling jets and for its pitch and yaw ACS jets is shown in Fig. 6. This plot indicates that the Ar in these jets supersaturates within one equivalent nozzle diameter and implies extensive condensation within the jet's nozzles.

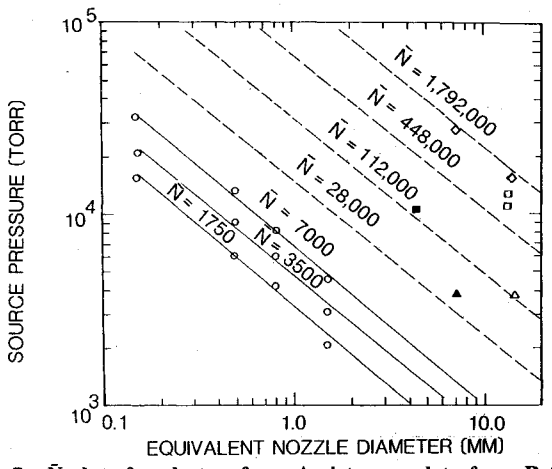

Fig. 7 $\bar{N}$ plots for clusters from Ar jets; o = data from Ref. 16; squares are source conditions for the target module argon jets, □ = pitch, yaw ACS, ■ = roll ACS ☑ = settling jet.

After illustrating that condensation of Ar in the ACS and settling jets is extremely likely, it is still necessary to predict the extent of condensation and the size of the particles formed by the condensation process. Unfortunately, we do not have sufficient theoretical understanding of homogeneous condensation processes for even simple substances such as Ar to accomplish this task. Fortunately, a number of experimental studies of Ar condensation are available on which to base estimates.

Once the onset of condensation is achieved, even to the extent of appreciable dimer and trimer formation, it is clear from molecular beam mass spectrometric studies of Ar cluster formation that a large fraction of the gas condenses. Studies by Milne and Greene[17,18] and Golomb et al.,[19] which probed only the onset of cluster formation, all showed that rapid Ar_x growth at the expense of monatomic Ar was characteristic of argon condensation. Once clusters containing more than ten argon atoms are formed, rapid agglomeration to large particles which can collect even more Ar atoms in single collisions is expected. Thus, if particles large enough to scatter visible and uv radiation effectively (100 Å or larger) can be formed in the jet expansion, it is likely that a large fraction of the jet flow (0.1 to 1.0) will be contained in the condensed particles.

In order to judge whether large Ar clusters are formed under MSMP jet conditions it is necessary to rely on the study of Hagena and Obert,[20] who have published the most extensive data on argon jet condensation. Hagena and Obert clearly demonstrate that the formation of a mean size condensation cluster $\bar{N}$ is characterized by simple products of source conditions raised to characteristic powers. The critical source parameters are T_0, P_0, and d_{eq}. For instance, using data from both sonic and conical nozzles, Hagena and Obert demonstrated that AR cluster size was proportional to $P_0^{1.7}$. They were also able to show tht for jets with $T_0 = 298$ deg, argon clusters of a given $\bar{N}$ were characterized by the

Table 2 Predicted argon jet cluster size and mass flux

	Ar Number (N)	Volume (V), cm^3	Diameter, μm	Mass flow, g/s	Cluster, s^{-1}
Target module					
Pitch, yaw	7.0×10^5	2.8×10^{-17}	0.038	311	6.73×10^{18}
Roll	1.2×10^5	4.8×10^{-18}	0.021	327	4.33×10^{18}
Settling	9.0×10^5	3.6×10^{-17}	0.042	347	5.84×10^{18}

relation[20]

$$P_0 d_{eq}^{0.8} = \text{constant} \tag{4}$$

Data illustrating Eq. (4) are shown in Fig. 7, where the open circles are data from Hagena and Obert for three mean cluster sizes as produced from a series of room temperature (298 K) sonic Ar jets. The dashed lines on Fig. 7 are extrapolated $\bar{N}$ values for higher source pressures and larger d_{eq} than those used by Hagena and Obert. The three noncircular symbols represent P_0 d_{eq} points for the three different argon jet conditions on the MSMP target module, as shown in Table 1. Since the source temperature for the jets is nominally also 298 K, estimates for the $\bar{N}$ (number of Ar atoms per mean size cluster) characteristic of the various argon jet conditions can be derived from Fig. 7. These estimated $\bar{N}$ are shown in Table 2. This table also includes calculated particle volumes, and diameters based on a solid argon density of 1.65 gm cm^{-3}.

While the particle sizes estimated from Fig. 7 are based on a severe extrapolation of available data, they are certainly worth a trial to determine if they can explain the MSMP visible and uv signals associated with the argon ACS and settling jets. To test this possibility, we have modeled the settling jet's signature observed at ~230 km and the pitch ACS jet signal observed at ~225 km.

Single-Particle Scattering Analysis

The scattering of electromagnetic radiation by a spherical argon cluster depends on only two parameters: 1) the refractive index of solid argon and 2) the ratio of the cluster perimeter to the photon wavelength. Given these two quantities, the intensity of the scattered radiation per unit incident flux may be calculated using Mie theory.[21]

The refractive index of solid argon has been measured by several investigators[22-24] with the result[23] that near the melting point and in the wavelength range from 0.36 to 0.65 μm the refractive index m decreases monotonically from 1.275 to 1.265. Based on the weak wavelength dependence of m, we have taken an average value of $m = 1.27$ (at all wavelengths) in our radiation predictions. A literature search revealed no information on the absorption index of solid argon; however, this index is proportional to the conductivity[21] of solid argon, which we take to be zero.

Given m, the scattering efficiency, Q_{scat}, of an argon cluster can be computed from the Mie theory as a function of the particle size parameter x. Consideration of the mean diameters given in Table 2, and the shortest wavelength of interest, the Lyman-α filter bandpass at 1216 Å, indicates that, in general, $x < 1$, so that an expansion of the Mie theory Q_{scat} about $x = 0$ that retains only the first term[21]:

$$Q_{scat} = \frac{8}{3} x^4 \left| \frac{m^2 - 1}{m^2 + 2} \right|^2 \tag{5}$$

was used. Equation (5) is the Rayleigh theory result.[21] For constant m, Eq. (5) predicts that the scattering efficiency varies as λ^{-4}.

The error associated with the use of Eq. (5), as opposed to the full Mie theory may be estimated by considering the predictions of both for the Lyman-α filter and the settling jet particle size. The Mie result is $Q_{scat} = 0.0803$, while the result of Eq. (5) is $Q_{scat} = 0.103$, or an overprediction of 29%. At the midpoint of HSP filter 1, 1575 Å, this overprediction has decreased to 14%, and the two predictions rapidly approach each other at longer wavelengths. The resulting calculated Q_{scat} values for the settling and pitch ACS jets of the target module are plotted in Fig. 8.

The intensity of radiation scattered per unit solid angle in the direction θ is[21]

$$S(\theta) = (3/16\pi)(1 + \cos^2\theta)\pi(D/2)^2 Q_{scat} I(\lambda) \tag{6}$$

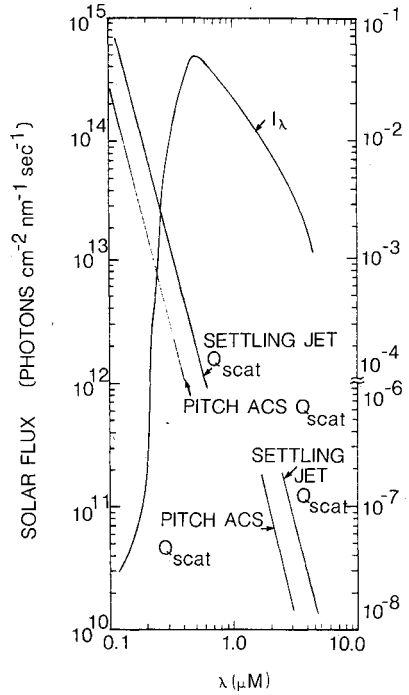

Fig. 8 Rayleigh scattering efficiency and solar flux.

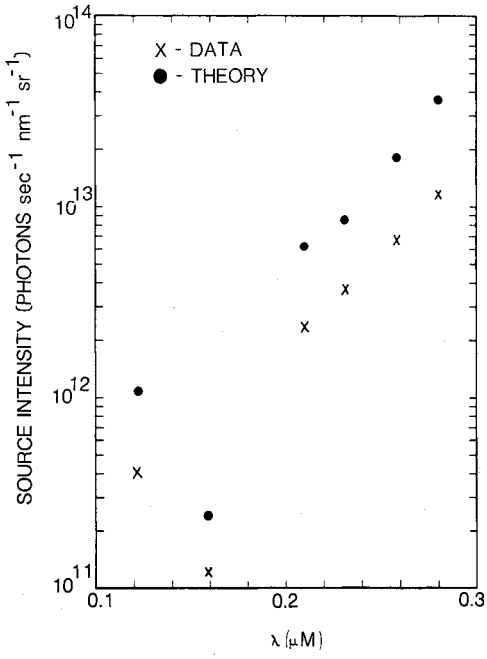

Fig. 9 Settling jet plume intensity.

where $I(\lambda)$ is the incident solar flux. The geometry of the MSMP flight was such that solar radiation scattered at $\theta = 90$ deg would strike the sensor module. As such, we have taken $\theta = 90$ deg in our modeling.

An important input in the solar scattering model is the solar flux in the 100-300-nm wavelength region. The spectrum used is a synthesis of spectra from three different sources.[25-27] From 100-120 nm, the recently measured solar irradiance of Hinteregger is used, while from 120-200 nm the data of Mount et al. is used, and above 200 nm the recommended fluxes in the COSPAR publication are used. Since this MSMP flight occurred near the solar maximum, the predicted plume solar scattering in the 100-200-nm region can be as much as a factor of 3 higher than that near the solar minimum. IR data were taken from Ref. 28. The approximate solar flux

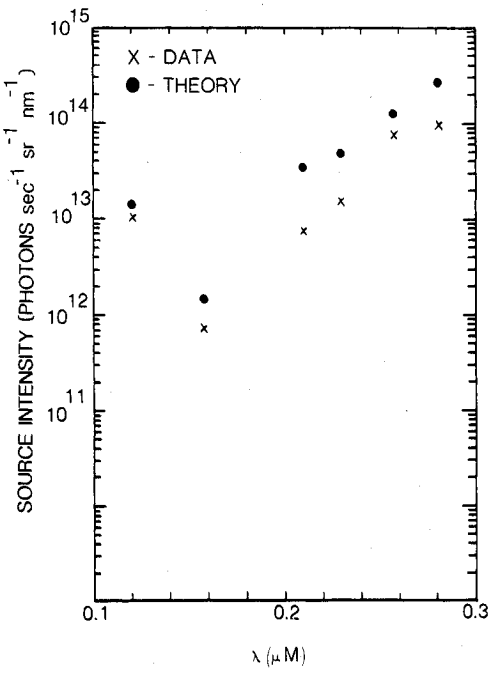

Fig. 10 ACS pitch plume intensity.

wavelength dependence is also illustrated in Fig. 8, cross-plotted for comparison with the calculated scattering efficiencies. The H atom Lyman-α flux is not indicated in this figure. The very low scattering efficiency in the IR, coupled with the relatively moderate solar flux explains why IR signals associated with target module argon jet activity were not observed by the IR instruments aboard the sensor module.

In the optically thin limit, all particles in the field-of-view (FOV) of a pixel contribute to the detector signal. As such, prediction of the scattered intensity from a given plume reduces to determining the number of clusters in the FOV of the detector followed by multiplication by Eq. (6). The number of clusters per unit length of plume depends both on the mass flow from a given jet and velocity of a cluster.

As discussed above, the visible and uv plume images have the structures of a high-altitude supersonic expansion. For this reason the density distribution of clusters produced by a jet is taken to be given by the Brook model[29]:

$$\rho(\bar{r}) = \frac{\rho_e A_e \xi^2}{2\pi r^2} \frac{V_e}{V_T} \exp[-\xi^2(1-\cos\phi)] \qquad (7)$$

Although developed for gas expansions, the Brook model will also describe the Ar cluster distribution if the condensation does not seriously perturb the expansion process.

The number of clusters in the pixels that contained the plume image was computed by integrating Eq. (7) both over the projected length of the plume image within the FOV of each photometer and over $0<\phi<60$ deg. This number then was combined with the results of Eq. (6), which predicts the intensity for a single cluster. The theoretical intensities are plotted in Figs. 9 and 10.

These predicted values may be compared with the experimental intensities in each bandpass, obtained, as noted above, from data like those shown in Figs. 4 and 5.

The predicted plume intensities all lie slightly above the data, which may be due to the assumption that all of the argon condenses, but is more likely due to our crude assumption of monodispersed droplets and uncertainty in the mean droplet size. In general, the agreement between MSMP data and the theoretical predictions based on an analysis of argon jet condensation and subsequent solar scattering is remarkable. It is clear that the cause of the ACS and settling jet related visible and uv interference has been identified.

Discussion

The fact that even a noble gas such as argon condenses under typical ACS jet conditions should really come as no surprise. Extensive literature exists on the use of jets to study condensation processes in gases.[30] In fact, even helium, with a boiling point of 4.3 K, has been observed to cluster under sufficiently severe freejet conditions.[31]

It is interesting to explore ways to avoid ACS jet induced visible and uv interference with sensitive optical observations conducted in sunlit orbits.

Three basic strategies for reducing the interfering signals are obvious: 1) change nozzle and chamber conditions to minimize condensation while maintaining thrust, 2) change propellants to prevent or minimize condensation while maintaining thrust, 3) change to a propellant that condenses, but is as transparent as possible, i.e., is a poor scatterer of solar radiation.

The particulate scattered signal is proportional to the product $Q_{scat}(\pi D^2/4)\,n$. If D is the average particle diameter, then [from Eq. (5)] $Q_{\rm scat}$ is proportional to D^4. Since the number of particles which can be formed from a given number of gas molecules is proportional to D^{-3}, then the scattered signal is proportional to $D^4 \times D^2 \times D^{-3}$, or D^3. Since the number of gas molecules in a condensed particle is also proportional to D^3, the scattered signal is directly proportional to $\bar{N}$, the number of gas molecules in the average particle.

Data for conical nozzles in Ref. 20 can be analyzed to show that $\bar{N}$ for argon is proportional to $P_0^{1.7}$, $T_0^{-4.0}$, and $(d\cot\eta)^{1.4}$ (Ref. 32). Thus option 1 involves using smaller, higher area ratio nozzles and/or heating the propellant. To reduce the scattered signal for an argon jet by a factor of 100, the propellant would have to be heated to 950 K, imposing severe weight, energy, and materials problems for most space systems.[32] Reduction of the nozzle diameter and opening up the nozzle area ratio would degrade the thrust characteristics too severely for most jet applications.

A more acceptable solution is to combine options 2 and 3 by selecting an optically inactive, low boiling point gas. Solid nitrogen has optical properties nearly identical to argon [$m_{N_2}=1.30\pm0.07$ (Ref. 24), $m_{\rm Ar}=1.275$ (Ref. 23)], while data on nitrogen condensation from Ref. 20 indicate that for similar nozzle conditions, $\bar{N}$ for nitrogen will be only about a factor of 4 smaller than $\bar{N}$ for argon.[32] Thus N_2 propelled jets will offer little reduction in scattered signal.

Helium would be the gas of choice to minimize $\bar{N}$, but unfortunately its low mass density means that a storage volume (at equal pressures) of 3.2 times that needed for either Ar or N_2 would have to be provided.

Neon appears to be the best compromise. Analysis of neon clustering data from Ref. 20 indicates that $\bar{N}$ for neon is 1/36 that of Ar under equivalent expansion conditions.[32] Furthermore, recent measurements of radiative lifetimes of 13 methyl-fluorine substituted benzene radical cations by Bondybey et al.[33] have shown that the average ratio of their radiative lifetime in solid neon matrices to the gas phase lifetime is only 1.135 ± 0.02 (Ref. 33), thus indicating that the refractive index of solid neon is 1.07 ± 0.02 (Ref. 34). Using Eq. (5) to compute the ratio of $Q_{\rm scat}$ for Ar, Ne, and N_2 at a fixed value of x indicates that while the scattering efficiency of a given particle size for N_2 is slightly greater than that for Ar, the scattering efficiency of the same size particle of Ne is only 0.07 of that for Ar.

When the reduction of $Q_{\rm scat}$ for neon (compared to argon) of 0.07 is combined with the reduction in $\bar{N}_{\rm Ne}/\bar{N}_{\rm Ar}$ of 1/36 or 0.028, a total reduction in scattered signal for equivalent nozzle flows of 0.002 is predicted. Thus a neon ACS jet should produce only about 1/500 the scattered visible and uv signal produced by an equivalent Ar jet. Neon jets should also be better than N_2 jets by a factor of roughly 100.

Furthermore, gaseous neon should be optically inactive under solar radiation at wavelengths longer than 774 Å.[35]

The major penalty for neon usage, besides the expense of purchase, is the need to provide 1.4 times the storage space (at a given pressure) to achieve the same impulse provided by Ar or N_2.[32]

Summary

Strong visible and uv signals due to solar scattering from space borne ACS jet plumes have been observed and analyzed. Condensed argon clusters with a mean diameter of 0.02 to 0.04 μm are shown to be responsible for this phenomenon.

Extrapolation of available laboratory condensation data for other jet propellant molecules indicated that nitrogen jets will produce solar scattered signals only slightly smaller than that for Ar. However, neon jets are predicted to produce visible and uv solar scattered signals at least 100 times below those for N_2 and Ar while maintaining reasonable propellant characteristics. Thus neon should be considered as an ACS jet propellant for space borne systems carrying sensitive visible or uv optical instruments.

Further laboratory data on the jet clustering kinetics and the condensed optical properties of neon, argon, and nitrogen are needed to refine the analysis reported here.

Acknowledgments

Work at Aerodyne Research, Inc. was supported by the Air Force Geophysics Laboratory under Contract F19628-78-C-0145. Useful technical discussions with M.E. Gersh, R.G. Steeves, T.A. Miller, M.B. McElroy, and J.L. Kerrebrock are gratefully acknowledged. The photometers were made by Martin Marietta Aerospace, Denver, Colo., and the digicon detectors were obtained from the Electron Vision Division of SAI, San Diego, Calif.

References

[1] Rieger, T.J., Tait, K.S., and Baum, H.R., "Atmospheric Interaction Radiation from High Altitude Rocket Exhausts," *Journal of Quantative Spectroscopy and Radiative Transfer,* Vol. 15, Dec. 1975, pp. 1117-1124.

[2] Rieger, T.J., Baum, H.E., Kolb, C.E., Tait, K.S., and Germeles, A.E., "Rocket Plume Radiation Due to Interactions with the Atmosphere, Volume I: Far Field Plume Radiance Model," Aerodyne Research, Inc., Billerica Mass., ARI-RR-36V.1, May 1973.

[3] Elgin, J.B., "Far Field Plume Interference Program," Aerodyne Research, Inc., Billerica, Mass., ARI-RR-102, March 1977.

[4] Curtis, J.T., Moselle, J.R., and Marrone, P.V., "Plume Interference Prediction (PIP) Code, Users Manual and Test Evaluation Report," Vol. 1, CALSPAN Corp., Buffalo, N.Y., KC-5100-A-6, April 1977.

[5] Curtis, J.T., Moselle, J.R., and Lordi, J.A., "PLUDAM; A Code for Calculating High Altitude Optic Sensor Interference from the Rocket Exhaust Plumes of Many Vehicles," CALSPAN Corp., Buffalo, N.Y., KC-6652-A-1, Aug. 1980.

[6] Simpson, J.P. and Witteborn, F.C., "Effect of the Shuttle Contaminant Environment on a Sensitive Infrared Telescope," *Applied Optics,* Vol. 16, Aug. 1977, pp. 2051-2073.

[7] Duff, J.W. and Bernstein, L.S., "Monte Carlo Scattering of Sunlight by High Altitude Rocket Plumes," *Journal of Quantitative Spectroscopy and Radiative Transfer,* Vol. 26, Jan. 1981, pp. 85-102.

[8] Kung, R.T.V., Cianciolo, C., and Meyer, J.A., "Solar Scattering from Condensation in Apollo Translunar Injection Plume," *AIAA Journal,* Vol. 13, April 1975, pp. 432-437.

[9] Wu, B.J.C., "Possible Water Vapor Condensation in Rocket Exhaust Plumes," *AIAA Journal,* Vol. 13, June 1975, pp. 797-802.

[10] Huffman, R.E., Paulsen, D.E., Larrabee, J.C., Baisley, V.C., LeBlanc, F.J., Frankel, D.S., and Gersh, M.E., "Vacuum Ultraviolet Airglow and Stellar Observations on the MSMP/TEM-1 Rocket Flight," Air Force Geophysics Laboratory, Bedford, Mass., AFGL-TR-80-0278, 1980.

[11] Russak, S.L., Flemming, J.C., Huffman, R.E., Paulsen, D.E., and Larrabee, J.C., "Development of Proximity and Electrostatically Focused Digicons for UV Measurements from Sounding Rockets," Air Force Geophysics Laboatory, Bedford Mass., AFGL-TR-79-0006, 1979.

[12] Wiese, W.L., Smith, M.W., and Miles, B.M., "Atomic Transition Probabilities," National Bureau of Standards, Washington, D.C., NSRDS-NBS-22, Vol. II, 1969.

[13] Lorents, D.C. and Olson, R.E., "Eximer Formation and Decay Processes In Rare Gases," Stanford Research Institute, Menlo Park, Calif., Report No. 1, Project PYU-2018, 1972.

[14] Koehler, H.A., Ferderber, L.J., Redhead, D.L., and Ebert, P.J., "Vacuum-Ultraviolet Emission from High-Pressure Xenon and Argon Excited by High-Current Relativistic Electron Beams," *Physical Review A,* Vol. 9, Feb. 1974, pp. 768-781.

[15] Anderson, J.B. and Fenn, J.B., "Velocity Distributions in Molecular Beams from Nozzle Flow," *Physics of Fluids,* Vol. 8, May 1965, pp. 780-787.

[16] Hagena, O.F., "Condensation in Supersonic Freejets," *Rarefied Gas Dynamics,* edited by L. Trilling, and H.Y. Wachman, Vol. II, Academic Press, New York, 1969, pp. 1465-1467.

[17] Milne, T.A. and Greene, F.T., "Mass Spectrometric Observations of Argon Clusters, in Nozzle Beams, I. General Behavior and Equilibrium Dimer Concentrations," *Journal of Chemical Physics,* Vol. 47, Nov. 1967, pp. 4095-5101.

[18] Milne, T.A. and Greene, F.T., "Mass Spectrometric Observations of Argon Clusters in Nozzle Beams, II. The Kinetics of Dimer Growth," *Journal of Chemical Physics,* Vol. 52, Feb. 1970, pp. 1552-1560.

[19] Golomb, D., Good, R.E., and Brown, R.F., "Dimers and Clusters in Free Jets of Argon and Nitric Oxide," *Journal of Chemical Physics,* Vol. 52, Feb. 1970, pp. 1545-1551.

[20] Hagena, O.F. and Obert, W., "Cluster Formation in Expanding Supersonic Jets: Effect of Pressure, Temperature, Nozzle Size and Test Gas," *Journal Chemical Physics,* Vol. 56, March 1972, pp. 1793-1802.

[21] Van De Hulst, H.C., *Light Scattering by Small Particles,* John Wiley & Sons, New York, 1957.

[22] Smith, B.L. and Pings, C.J., "Refractive Index of Solid Argon," *Physica,* Vol. 29, May 1963, p. 255.

[23] Sinnock, A.C. and Smith, B.L., "Dielectric Properties of the Solidified Inert Gases," *Physics Letters (The Netherlands),* Vol. 28A, Oct. 1968, pp. 22-23.

[24] Gibson, E.P. and Rest, A.J., "The Determination of the Refractive Indices of Frozen Gas Matrices at 12 K by Emission Spectroscopy," *Chemical Physics Letters,* Vol. 73, July 1980, pp. 294-296.

[25] Hinteregger, H.E., Air Force Geophysics Laboratory, private communication.

[26] Delaboudiniere, J.P., Donnelly, R.F., Hinteregger, H.E., Schmidtje, G., and Simon, P.C., "Intercomparison/Compilation of Relevant Solar Flux Data Related to Aeronomy," COSPAR Technique Manual Series No. 7, 1978.

[27] Mount, G.H., Rottman, G.J., and Timothy, J.G., "The Solar Spectral Irradiance 1200-2550 Å at Solar Maximum," *Journal of Geophysical Research,* Vol. 85, Aug. 1980, pp. 4271-274.

[28] Valley, S.L. (ed.), *Handbook of Geophysics and Space Environments,* McGraw-Hill, New York, Chap. 16.

[29] Brook, J.W., "Far Field Approximation For a Nozzle Exhausting into a Vacuum," *Journal of Spacecraft and Rockets,* Vol. 6, May 1969, p. 626.

[30] Wegener, P.P. and Wu, B.J.C., "Gas Dynamics and Homogeneous Nucleation," *Advances in Colloid and Interface Science,* Vol. 7, 1977, pp. 325-417.

[31] Van Deursen, A.P.J. and Reuss, J., "Experimental Investigation of Small He Clusters," *Journal of Chemical Physics,* Vol. 63, Nov. 1975, pp. 4559-4560.

[32] Elgin, J.B., "Progress in High Altitude Radiation Studies," Physical Sciences, Inc., Woburn, Mass., TR-256, 1981.

[33] Bondybey, V.E., Vaughn, C., Miller, T.A., English, J.H., and Shiley, R.H., "Spectroscopy and Decay Dynamics of Several Methyl and Fluorine Substituted Benzene Radical Cations," *Journal of the American Chemical Society,* Vol. 103, Oct. 1981, pp. 6303-6307.

[34] Olmsted, J., "Effect of Refractive Index on Molecular Radiative Lifetimes," *Chemical Physics Letters,* Vol. 38, March 1976, pp. 287-299.

[35] Wiese, W.L., Smith, M.W., and Glennon, B.M., "Atomic Transition Probability, Vol. I, Hydrogen Through Neon," National Bureau of Standards, Washington, D.C., NSRDS-NB5-4, 1968.